Manganese(ii) thiophosphate (MnPS3) intercalates with lanthanide (Pr-III and Nd-III) complexes: optical and magnetic properties

Pablo Fuentealba, Jeannette Morales, Nathalie Audebrand, Claudio José Magon, Hellmut Eckert, Jorge Manzur, Evgenia Spodine

Graphical Abstract

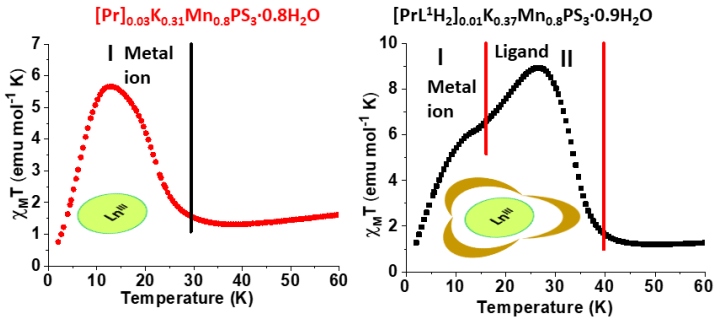

Intercalation of 4f species into manganese(II) thiophosphate host.

Manganese(II) Thiophosphate ($MnPS_3$) Intercalates with Lanthanide (Pr^{III} and Nd^{III}) Complexes: Optical and Magnetic Properties

Pablo Fuentealba[a]*, Jeannette Morales[a], Nathalie Audebrand[c], Claudio José Magon[d], Hellmut Eckert[d], Jorge Manzur[a], Evgenia Spodine[a,b]*

[a] Dr. P. Fuentealba, M.Sc. J. Morales, Prof. J. Manzur, Prof. E. Spodine.
Facultad de Ciencias químicas y Farmacéuticas, Departamento de Química Inorgánica y Analítica
Universidad de Chile
Olivos 1007, Independencia, Santiago, Chile
E-mail: pfuentealbacastro@ciq.uchile.cl; espodine@ciq.uchile.cl

[b] Prof. E. Spodine.
Centro para el Desarrollo de la Nanociencia y Nanotecnología (CEDENNA)
Avda. Libertador Bernardo O'Higgins 3363, Estación Central, Santiago, Chile.

[c] Prof. Nathalie Audebrand
Univ Rennes, INSA Rennes, CNRS, ISCR (Institut des Sciences Chimiques de Rennes)
UMR 6226, F-35000, Rennes, France

[d] Prof. C. J. Magon, Prof. H. Eckert
Instituto de Física de São Carlos
Universidade de São Paulo
13566-590 São Carlos, SP, CP 369, Brazil.

Supporting information for this article is given via a link at the end of the document.

Abstract: We report the intercalation of Pr^{III} and Nd^{III} macrocyclic complexes into the layered hexahypothiophosphate $MnPS_3$ and the effect of this process on the optical and magnetic properties of the layered host. Spontaneous magnetization is observed within the 20-40 K temperature range, arising as a consequence of vacancy ordering occurring in the antiferromagnetically coupled host material. The band gap energy values are also modified, all intercalates showing lower values as compared to the pristine phase. Both effects are remarkably sensitive to the nature of the guest species, suggesting an interaction of the organic ligand with the terminal sulfur atoms of the $P_2S_6^{4-}$ ions.

Introduction

The family of transition metal thiophosphates (TMTPs) were reported many years ago and are still under research due to their intruiguing properties. They form 2D layered structures, in which anionic $P_2S_6^{4-}$ units are charge-compensated by divalent metal cations. Depending on the cation present, the type of bonding between these species ranges from highly ionic to strongly covalent. Six sulfur atoms bound to each metal center give rise to a slightly distorted octahedral environment, while the $P_2S_6^{4-}$ anions have an ethane like structure. The formed layers are held together by weak van der Waals interactions. The interlayer space can accommodate different atomic and molecular species [1–3], resulting in intercalation compounds with drastically altered optical and magnetic properties.

TMTPs were originally reported in the 1970-s [4–8], and were largely studied until the end of the twentieth century [9–13], due to their different functionalities, such as semiconducting, gas storage, and catalytic properties, among others [14,15]. Furthermore, the pristine TMTPs, (MPS_3 or $MPSe_3$) and some bimetallic phases such as $CuBiP_2Se_6$, have band gaps ranging from 1.2 to 3.5 eV, and some of them present ionic conductivity [2,16]. Since these phases are good candidates for new applications in the electronics field, the interest for these materials is re-emerging [2,17]. A well known intermediate to do further intercalation reactions is the potassium precursor (PP) $K_{0.4}Mn_{0.8}PS_3{\cdot}H_2O$, which is obtained by simply immersing the pristine phase in a 2M KCl solution for 24 hours [18–22]. This intercalated phase can then be used as a precursor for the partial ion exchange of the interlayer potassium ions by more voluminous guests, such as coordination compounds [23]. All these reactions give rise to intercalation compounds with different optical, electrical, and magnetic properties. While $MnPS_3$ is known to be a semiconductor with a band gap of 2.5 eV and antiferromagnetic properties showing a broad maximum of the magnetic susceptibility at 120 K, typical of a low dimensional magnetic system, the potassium intercalated compound (PP) has a band gap of 2.65 eV and shows spontaneous magnetization at 16 K. This magnetic phenomenon is attributed to vacancy ordering in the layers, due to the partial migration of Mn^{II} ions from the

layer when potassium ions are intercalated into the interlamellar space [24,25]. Moreover, using the PP as an intermediate, nanocomposites have been obtained with transition metal complexes intercalated in the above mentioned interlamellar space [26]. These materials have lower band gap values than either PP or the pristine $MnPS_3$ phases, and the magnetic properties are also modified. The intercalates show a more complex magnetic behavior than PP or $MnPS_3$, evidencing the influence of the guest species on the optical and magnetic properties [18–20,26].

Among the different reported species intercalated in PP, lanthanide(III) ions and their corresponding complexes have not been widely used as guests in intercalates of $MnPS_3$. On the other hand, bimetallic phases containing lanthanide(III) cations have been reported [17,27]. In this work, we report the optical and magnetic properties of novel compounds based on the $MnPS_3$ phase intercalated with lanthanide(III) cations from nitrate salts, and the corresponding cationic macrocyclic complexes, derived from $(ML^nH_2)(NO_3)_3(H_2O)_x$, M: Pr^{III} and Nd^{III}. The macrocyclic complexes were prepared by the template condensation reaction of 2-hydroxy-5-methyl-1,3-benzenedicarbaldehyde and two different amines, *o*-phenylenediamine (L^1H_2) or 1,3-diaminepropane (L^2H_2).

Results and Discussion

The above described intercalation reaction of $K_{0.4}Mn_{0.8}PS_3{\cdot}H_2O$ with Pr^{III} and Nd^{III} complexes, using the microwave assisted ion exchange reaction, produced the following intercalation compounds: $[PrL^1H_2]_{0.01}K_{0.37}Mn_{0.8}PS_3{\cdot}0.9H_2O$ (***1***) and $[NdL^1H_2]_{0.01}K_{0.37}Mn_{0.8}PS_3{\cdot}0.9H_2O$ (***2***); $[PrL^2H_2]_{0.05}K_{0.25}Mn_{0.8}PS_3{\cdot}0.9H_2O$ (***3***) and $[NdL^2H_2]_{0.05}K_{0.25}Mn_{0.8}PS_3{\cdot}0.9H_2O$ (***4***). In addition $[Pr]_{0.03}K_{0.31}Mn_{0.8}PS_3{\cdot}0.8H_2O$ (***5***) and $[Nd]_{0.03}K_{0.31}Mn_{0.8}PS_3{\cdot}0.8H_2O$ (***6***) were obtained using the lanthanide(III) nitrate salts instead of the macrocyclic complexes. The stoichiometry was established using SEM-EDXS and ICP data. Both techniques provided similar results. As observed in the SEM-EDX diagrams the exchange is not complete, since the data give clear evidence of potassium ions (Figure S1). The ionic exchange was done using a 1:3 lanthanide nitrate (or macrocyclic complex) to potassium ratio. This ratio was selected since the macrocyclic complexes are intercalated as cationic $[ML^nH_2]^{3+}$ species, or as hydrated lanthanide(III) cations. Both $[Pr(NO_3)_3(H_2O)_4]{\cdot}2H_2O$ and $[Nd(NO_3)_3(H_2O)_4]{\cdot}2H_2O$ are ten- coordinated species, in which the first coordination sphere is formed by three bidentate nitrate ions and four water molecules, while the remaining two water molecules are situated in the lattice [28,29]. The lanthanide(III) ions in the corresponding macrocyclic complexes are reported to be also tenfold coordinated. Besides the macrocyclic ligand, which acts as a N_2O_2 donor, three bidentate nitrate ligands complete the coordination sphere [30]. Thermal gravimetric analysis (TGA) data (Figure S2) indicate distinct weight loss temperature regimes: an 8% weight loss below 100 °C, attributed to molecular water within the interlayer spaces. A subsequent gradual ~ 6-10% weight loss between 100-400 °C in the case of ***(1)*** and ***(2)***, and between 100 and 500°C in the case of ***(3)*** and ***(4)*** is partially attributed to ligand decomposition. This decomposition step is absent in ***(5)*** and ***(6),*** reflecting the absence of organic ligands in the latter intercalates. In all six compounds host decomposition is indicated by the high-temperature weight loss step above 600-650°C. FTIR spectra of these intercalation compounds are dominated by the typical double absorption band centered at 572 and 608 nm, assigned to the PS_3 vibration, the splitting of which is indicative of the existence of the previously formed vacancies in the layers of the PP [32]. Furthermore, there are no bands due to nitrate counterions, which are observed at *ca.* 1300 cm^{-1} (ν_3 antisymmetric stretching mode) and 1050 cm^{-1} (ν_1 symmetric stretching mode) in the spectra of the complexes and nitrate salts [30]. Reports from literature indicate that the nitrate ions can be easily removed from the first coordination sphere [31] (Figures S3b and S3c); therefore, the FTIR spectra are consistent with the intercalation of the complexes as cationic species. Finally, weak bands due to low concentration of the macrocyclic ligands are observed in the 1600-800 cm^{-1}spectral region. The X-ray diffraction patterns of all the intercalates have a sharp 001 reflection at a 2θ value of 9.2˚, corresponding to an interlayer distance of 9.6 Å (Figure S4). By modelling the XRD data with a Le Bail fit it is possible to index all the diffraction lines and to obtain the unit cell parameters (Figure S4 and Table S1). The interlayer distance is comparable to that measured for the potassium intercalate precursor $K_{0.4}Mn_{0.8}PS_3{\cdot}H_2O$, which is understandable as the materials retain a significant amount of potassium. [18] Based on the dimensions of the macrocyclic complexes (Figure S5) and the experimental interlamellar distance, we conclude that the guest macrocycle is oriented parallel to the layers of the host, making viable the interactions through the lanthanide cations and/or the π–cloud of the ligands with the protruding sulphur atoms.

Figure 1 presents the absorption spectra of the studied intercalation compounds and the potassium precursor. The obtained band gap energy values, calculated from the corresponding Taul plots (Figure S6), of the intercalated compounds with complex species are lower than the values for $K_{0.4}Mn_{0.8}PS_3{\cdot}H_2O$ (2.65 eV) and $MnPS_3$ (2.50 eV, Table 1). While (***1***) and (***2***) have similar band gap values of 1.87 and 1.85 eV, (***3***) and (***4***) show an increased band gap of 2.21 eV [20]. Furthermore, the band gap energy values for $[Pr]_{0.03}K_{0.31}Mn_{0.8}PS_3{\cdot}0.8H_2O$ (***5***) and $[Nd]_{0.03}K_{0.31}Mn_{0.8}PS_3{\cdot}0.8H_2O$ (***6***) are 2.26 and 2.29 eV, respectively.

The intercalated compounds with macrocyclic complexes have lower band gap values than the ones derived from nitrate salts. Within these intercalates, those with L^1H_2 present the lowest values. This ligand has a more rigid structure with more delocalization, as compared to L^2H_2, enhancing the interaction with the lamellae. The obtained data show that the ligand plays a significant role in the modification of the optical properties. The electronic interaction between ligand and the terminal S atoms of the lamellae is evident from the fact that the spectra of the intercalation compounds differ significantly from those of a physical mixture of $K_{0.4}Mn_{0.8}PS_3{\cdot}H_2O$ and the Ln(III) coordination compounds.

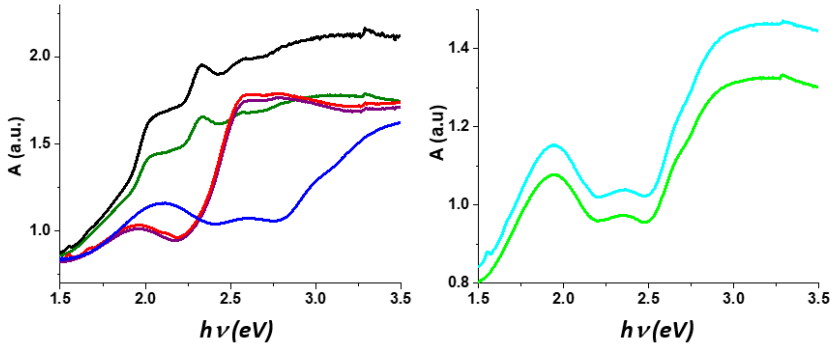

Figure 1. Absorption spectra of: (left) the potassium precursor (blue) and intercalates with complexes (***1***) (green), (***2***) (black), (***3***) (purple) and (***4***) (red); (right) absorption spectra of (***5***) (light green), and (***6***) (light blue), obtained from the nitrate salts.

Table 1: Band gap energy values for the studied phases.

Compound		Energy gap (eV)
$MnPS_3$	**TMTP**	2.50
$K_{0.4}Mn_{0.8}PS_3{\cdot}H_2O$	**PP**	2.65
$[PrL^1H_2]_{0.01}K_{0.37}Mn_{0.8}PS_3{\cdot}0.9H_2O$	***(1)***	1.87
$[NdL^1H_2]_{0.01}K_{0.37}Mn_{0.8}PS_3{\cdot}0.9H_2O$	***(2)***	1.85
$[PrL^2H_2]_{0.05}K_{0.25}Mn_{0.8}PS_3{\cdot}0.9H_2O$	***(3)***	2.21
$[NdL^2H_2]_{0.05}K_{0.25}Mn_{0.8}PS_3{\cdot}0.9H_2O$	***(4)***	2.21
$[Pr]_{0.03}K_{0.31}Mn_{0.8}PS_3{\cdot}0.8H_2O$	***(5)***	2.26
$[Nd]_{0.03}K_{0.31}Mn_{0.8}PS_3{\cdot}0.8H_2O$	***(6)***	2.29

This fact can be rationalized by assuming that the protruding sulfur atoms of the lamellae interact with the intercalated species, and this phenomenon alters the energy levels that give rise to the band gap energy value. The reported ionic model that describes the transitions in $MnPS_3$ defines the band gap as the electronic transition between the valence band and the conduction band states. The former is mainly constructed from $3p_z$(P-P) orbitals, while the latter is predominantly associated with anti-bonding orbitals $3p_z^*$ (S) [33]. Upon intercalation, the $3p_z^*$(S) state energy may be lowered, resulting in an observed lower band gap energy value.

The magnetic properties of the materials are also affected by the presence of the lanthanide (III) ions, and of the corresponding complexes present in the interlayer space of these intercalates.

As already stated, the potassium precursor has vacancies and these have been proven by neutron and X-ray diffraction to be ordered within the individual lamellae [24,25]. This ordering is important to explain the magnetic structure. If the vacancies are situated either on the “spin up” or “spin down” sites, then the antiferromagnetic ordering is broken and the intercalate exhibits a bulk spontaneous magnetization at low temperatures, corresponding to ferromagnetic ordering. Therefore, a drastic modification of the magnetic properties takes place, and a net spontaneous magnetization at 16 K is observed in PP, the intercalated $MnPS_3$ phase with hydrated potassium ions [24].

The materials obtained by intercalation of the lanthanide(III) complexes into the PP also show a spontaneous magnetization, confirming that the vacancies still exist in the new materials. Figure 2a shows the $\chi T(T)$ curves for the original PP and PP after MW irradiation, showing that the latter does not affect the magnetic behaviour of PP. Figures 2b and 2c show the magnetic behaviour of the Pr^{III} – based intercalates (*1*) and (*3*), respectively. The curves for the Nd^{III} – based intercalates (*2*) and (*4*) have similar profiles (Figure S7a and S7b, respectively). In general the χT versus T curves show two maxima near 10-15 K and 25-30 K. In the intercalation compound of the complex with the ligand L^1H_2, derived from the aromatic amine (*o*-phenylenediamine), the second maximum is more intense (Figure 2b), while

in the intercalation compound of the complex with the L^2H_2 ligand, derived from the aliphatic amine (1,3-diamine) the two maxima are about equally intense (Figure 3c). In contrast, the data for the compounds intercalated with simple lanthanide(III) ions show only a single χT maximum near 15 K, see Figure 2d and Figure S7c.

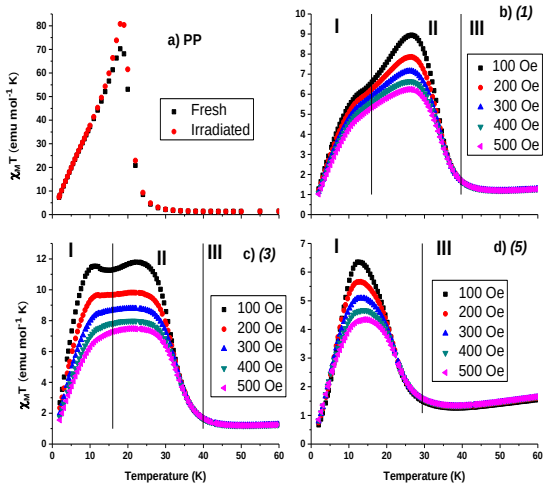

Figure 2. Temperature dependence of the χT product in the temperature range 2-60 K at different magnetic fields. a) $K_{0.4}Mn_{0.8}PS_3{\cdot}H_2O$ (PP), b) $[PrL^1H_2]_{0.01}K_{0.37}Mn_{0.8}PS_3{\cdot}0.9H_2O$ ***(1)***, c) $[PrL^2H_2]_{0.05}K_{0.25}Mn_{0.8}PS_3{\cdot}0.9H_2O$ ***(3)***, and d) $[Pr]_{0.03}K_{0.31}Mn_{0.8}PS_3{\cdot}0.8H_2O$ ***(5)***. Roman numbers I, II and III denote temperature ranges, as described in the text.

The comparison between all of these curves of compounds (***1***) to (***6***) suggests that in all intercalates the presence of vacancies in the layer is responsible for the spontaneous magnetization, and this phenomenon can be influenced by the nature of the different intercalated species. The maxima near *ca.* 30 K, (or, in the temperature region II denoted in Figure 3) characterize the influence of the organic ligands on the Mn^{II} cations, whereas the maxima at the lower temperatures (*ca.* 12 K, or, in the temperature region I denoted in Figure 2), reflect the effect of the rare-earth metal centers. Specifically, their interaction with the protruding sulfur atoms of the layers affects the ordering temperature of the obtained compounds.

As suggested by the relative intensities of the maxima at 30 K of the $\chi T(T)$ curves, the aromatic moieties of L^1H_2 interact with the protruding sulfur atoms more strongly than the aliphatic moieties of L^2H_2. Region III corresponds to higher temperatures where spontaneous magnetization ordering does not take place.

We conclude that the magnetic behaviour at low temperatures is strongly dependent on the nature of the macrocyclic ligand, and less dependent on the nature of the lanthanide(III) ion. This was corroborated further by the comparison with the magnetic susceptibility curve of a dinuclear copper(II) complex intercalate, with L^1H_2 as ligand; $[Cu_2L^1]_{0.08}K_{0.24}Mn_{0.8}PS_3$, which shows the same profile as (***1***) and (***2***) (Figure 3).

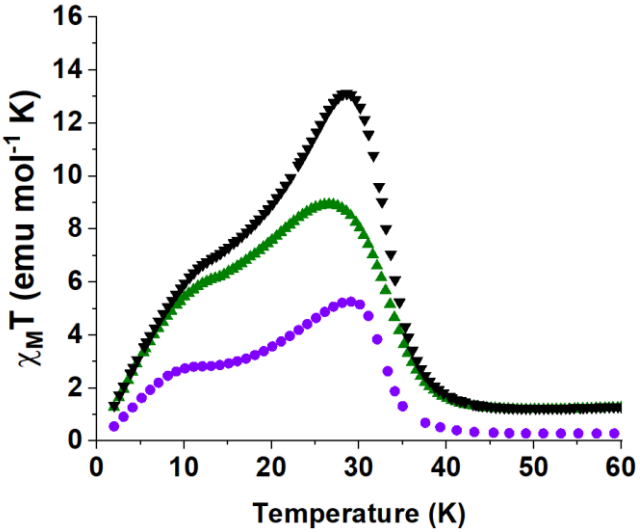

Figure 3. Comparison of the temperature dependence of $\chi T(T)$ of ***(1)*** (green triangle), ***(2)*** **(**black inverted triangle) and a dinuclear copper(II) complex based intercalate,$[Cu_2L]_{0.08}K_{0.24}Mn_{0.8}PS_3$, (violet circles).

Table 2. Weiss constants (θ) of the obtained intercalated compounds

Formula	θ (K)
$MnPS_3$	-250[25]
$K_{0.4}Mn_{0.8}PS_3{\cdot}H_2O$	-100[18]
$[PrL^1H_2]_{0.01}K_{0.37}Mn_{0.8}PS_3{\cdot}0.9H_2O$ ***(1)***	-193
$[NdL^1H_2]_{0.01}K_{0.37}Mn_{0.8}PS_3{\cdot}0.9H_2O$ ***(2)***	-205
$[PrL^2H_2]_{0.05}K_{0.25}Mn_{0.8}PS_3{\cdot}0.9H_2O$ ***(3)***	-115
$[NdL^2H_2]_{0.05}K_{0.25}Mn_{0.8}PS_3{\cdot}0.9H_2O$ ***(4)***	-125
$[Pr]_{0.03}K_{0.31}Mn_{0.8}PS_3{\cdot}0.8H_2O$ ***(5)***	-114
$[Nd]_{0.03}K_{0.31}Mn_{0.8}PS_3{\cdot}0.8H_2O$ ***(6)***	-133

Furthermore, in order to further characterize the observed spontaneous magnetization, the corresponding hysteresis loops were recorded. All the intercalates present a hysteresis loop at 2K (Figure S8), corroborating the presence of a ferromagnetic phenomenon in the intercalates.

Table 2 summarizes the Weiss constant (θ) values, extracted from the high temperature range (150-300 K, as shown in figure S9) of the χ^{-1} versus T curves, obtained for an external magnetic field of 100 Oe. All these intercalates, including PP, show a weaker antiferromagnetic (AF) character than the pristine phase, $MnPS_3$.

Thus the PP phase is the one with the weakest bulk antiferromagnetic interaction, while the intercalation compounds based on Pr^{III} ($4f^2$) complexes (***1***), (***3***) and (***5***), have less AF character, as compared to the Nd^{III} ($4f^3$) ones (***2***), (***4***) and ***(6)*** (Table 2). If only the vacancies were responsible for the modification of the magnetic properties of PP and the studied intercalates, then the AF nature would have been the same in all the systems, since the number of vacancies remains constant. Due to the fact that the lanthanide cations and complexes have a greater volume than the Mn^{II}

vacancies, the number of vacancies is not modified, and it becomes evident that interactions between the $MnPS_3$ layers with the paramagnetic lanthanide species situated within the interlayer space play a role in modifying the magnetic properties.

AC susceptibility measurements were carried out for all the studied systems (Figure S10). In order to have a better comparison of the magnetic dc and ac data, Figure 4 depicts the χ_M, χ' and χ'' curves for $[PrL^1H_2]_{0.01}K_{0.37}Mn_{0.8}PS_3{\cdot}0.9H_2O$ ***(1)*.**

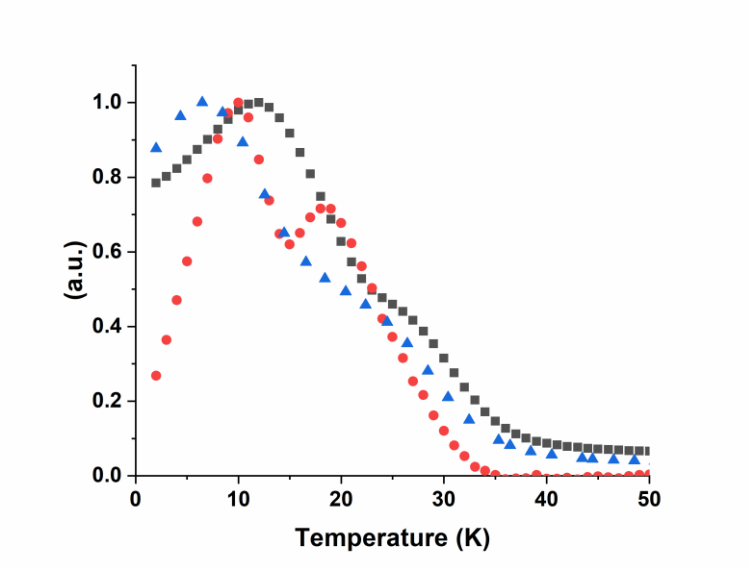

Figure 4: Normalized dc magnetic susceptibility (χ_M blue triangles), in phase magnetization (χ', black squares) and out of phase magnetization (χ'' red spheres) for $[PrL^1H_2]_{0.01}K_{0.37}Mn_{0.8}PS_3{\cdot}0.9H_2O$ ***(1)***.

The existence of peaks in the in-phase component of the ac susceptibility (χ') evidences a magnetic phase transition to an ordered state. The observation of maxima in the imaginary part of the ac susceptibility (χ'') can be explained by the existence of a partially canted antiferromagnetic structure that generates a weak ferromagnetic response in the sample.

For intercalates (***1***) and (***2***), in the absence of an external *dc* field, the dynamic magnetic measurement data present two distinct out-of-phase signals, χ'' at *ca.* 10 and 20 K. However, when an external field of 100 Oe is applied the second maximum becomes less intense. For (***3***) and (***4***) only one maximum is detected for χ'' at *ca.* 15 and 22 K for 100 Oe and zero dc field, respectively, being independent of the nature of the central ion. When the external field is applied the intensity of this maximum is also decreased, as for (***1***) and (***2***). Finally, for (***5***) and (***6***) only one signal is detected at *ca.* 10 K for both intercalates, whether 100 Oe of external field is applied or in the absence of a magnetic field. This permits to conclude that when the intercalate is only formed by the lanthanide cations (Pr^{III} or Nd^{III}) the magnetic ordering is present, independent of the existence or not of an external field. Moreover, the materials formed by the insertion of the lanthanide complexes have ordering temperatures that are dependent on the nature of the used macrocyclic ligand. These findings corroborate the data obtained by *dc* measurement, suggesting an influence of the interlayer interactions of the sulphur atoms with intercalated cations and macrocyclic ligands upon the magnetic ordering behaviour.

The influence of the aromatic macrocyclic ligand on the optical and magnetic properties was further investigated by recording EPR data for ***(1), (2), (5)*** and ***(6)***. The obtained spectra for the Pr^{III}-based intercalation compounds are shown in Figure 5. Results on the Nd^{III}-based intercalation compounds were very similar and are shown in Figure S11a and S11b. All of these spectra arise from the Mn^{II} ions (d^5) interacting with their local environments.

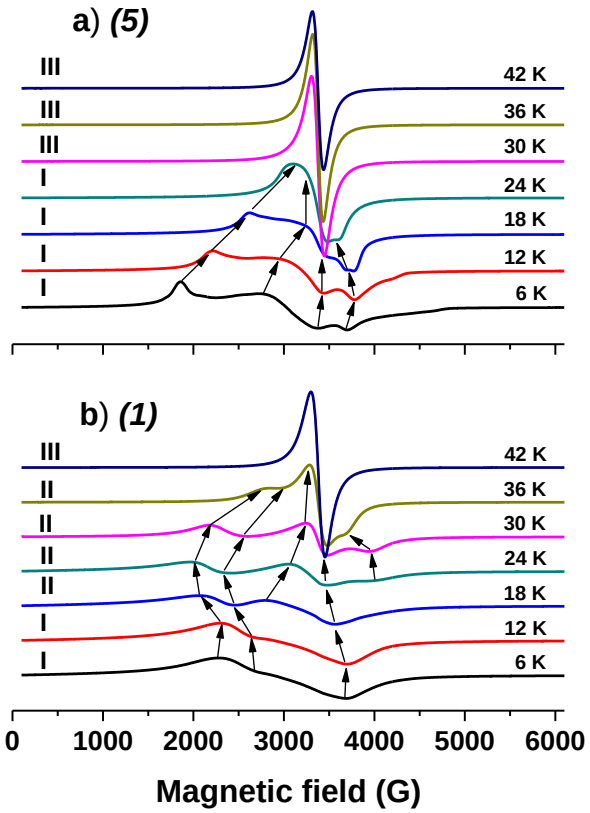

Figure 5. EPR spectra at selected temperatures for ***(5)*** (a) and ***(1)*** (b). Arrows are guides to the eyes to show the evolution of the main spectral features as a function of temperature. Roman numbers I, II and III denote temperature ranges, as described in the text. Microwave frequency: 9.442 GHz.

In recent reports we have described the EPR analysis for $MnPS_3$ and $K_{0.4}Mn_{0.8}PS_3$ [18,21]. Due to the high concentration of Mn(II) ions the magnetic hyperfine interaction with the ^{55}Mn (I=5/2) nuclei is not observed owing to exchange narrowing. The pristine phase shows a single line in the whole temperature range attributed to the M_s = -1/2 <-> M_s = +1/2 transition of the zero-field split resonance. In contrast, PP shows a single line only at temperatures above 20K, while presenting a broad and structured spectrum in the low temperature range where the magnetic measurements reveal spontaneous magnetization. Here, the broader and structured spectra reflect the effect of vacancies in the layer, which modifies the environment of some of the paramagnetic cations, creating Mn^{II} sites experiencing a distribution of local magnetic fields of different magnitudes.

The spectra of the intercalation compounds of the present study, shown in Figure 5, reveal similar behaviour as that of the potassium precursor [18]: structured spectra are observed in the spontaneous magnetization temperature range, while exchange-narrowed spectra, with g-values close to 2, are seen in the paramagnetic Curie-Weiss regime above ca. 40 K (region III). Attempts to simulate these spectra, by using the usual spin Hamiltonian parameters characterizing the Zeeman and zero-field splitting interactions, could not reproduce the experimental data satisfactorily. Therefore, we conclude that such broad spectra observed at low temperatures (regions I and II) must be a result of the presence of different static local internal magnetic fields at the Mn^{II} sites, due to the spontaneous magnetization regime. However, to prove this hypothesis, further field-dependent experiments with different microwave sources will be needed.

For a qualitative assessment, we can correlate the temperature dependent line shapes with the magnetic behaviour of the different intercalation compounds examined in this study. For compounds ***(5)*** and ***(6)***, intercalated with simple lanthanide cations from nitrate salts, we observe broad and structured spectra at 6K. Temperature increase leads to a

narrowing of the spectra, with a complete monotonic collapse into a single line *ca.* 30K. This behaviour resembles the one of the potassium precursor. On the other hand, the spectra of the compounds ***(1)*** and ***(2),*** intercalated with the macrocyclic complexes derived from 2-hydroxy-5-methyl-1,3-benzenedicarbaldehyde and the aromatic amine, 1,2-phenylenediamine, show a much more complex temperature dependence. A broad spectrum is observed in region I, between 6-12 K; however, as the temperature is increased in region II the spectrum gets even broader. Finally, narrowing into a single line is observed only above 36 K. Such different behaviour between samples ***(1)*** and ***(2)*** on one hand, and ***(5)*** and ***(6)*** on the other can be related to the wider temperature range of the spontaneous magnetization for samples ***(1)*** and ***(2)*** (Figure 2). Similar results have been described for intercalates with macrocyclic complexes with *3d* ions [18], and for those containing only organic molecules [34]. We thus conclude that the phenomenon observed in the range of 20-30 K (region II) must be related to the influence of the organic molecule or ligand present in the intercalate, while the phenomenon observed below 20K (region I) should be related to the influence of the metallic cation.
The fact that the Pr^{III} complex intercalates show similar EPR results to those of the Nd^{III} complex intercalates, and that the intercalates with simple lanthanide(III) cations show similar EPR results to those of the potassium precursor, confirms the conclusion based on the magnetic susceptibility. That is, the nature of the *4f* cations plays a less significant role in determining magnetic properties than the interaction of the protruding sulfur atoms with the organic ligand of the complexes.

Conclusion

The intercalation compounds $[PrL^1H_2]_{0.01}K_{0.37}Mn_{0.8}PS_3{\cdot}0.9H_2O$ (***1***) and $[NdL^1H_2]_{0.01}K_{0.37}Mn_{0.8}PS_3{\cdot}0.9H_2O$ (***2***), $[PrL^2H_2]_{0.05}K_{0.25}Mn_{0.8}PS_3{\cdot}0.9H_2O$ (***3***) and $[NdL^2H_2]_{0.05}K_{0.25}Mn_{0.8}PS_3{\cdot}0.9H_2O$ (***4***), $[Pr]_{0.03}K_{0.31}Mn_{0.8}PS_3{\cdot}0.8H_2O$ (***5***) and $[Nd]_{0.03}K_{0.31}Mn_{0.8}PS_3{\cdot}0.8H_2O$ (***6***) were obtained using the microwave-assisted ion exchange reaction of $K_{0.4}Mn_{0.8}PS_3{\cdot}H_2O$. The intercalation process greatly affects the optical and magnetic properties of the intercalates, especially those obtained with the macrocyclic complexes based on L^1H_2. Reflectance spectra indicate that there is a substantial decrease in the band gap energy. Weiss constants extracted from magnetic susceptibility measurements indicate that the antiferromagnetic interactions of the host compound are weakened in the PP intercalate and further modified by the intercalation oft he rare earth ions and their complexes. Moreover, due to an ordered array of vacancies in the layers, the intercalates including PP present spontaneous magnetization at low temperatures. However, the spontaneous magnetization is not only due to the parallel orientation of the magnetic dipoles around the vacancies in the layers of $MnPS_3$, but is also influenced by the interaction of the intercalated guest species with the sulphur atoms of the layers. All the data point to the fact that the interaction most relevant above 15 K is between the ligand and the protruding sulfur atoms.

Experimental Section

Reagents and Equipments.
Solvents were distilled before each reaction, while diamines, potassium chloride and lanthanide(III) nitrates were used as received from Sigma-Aldrich. 2-hydroxy-5-methyl-1,3-benzenedicarbaldehyde was synthesized, using the protocol described by Papadopoulos *et al.* [35] and purified by sublimation. Pure elemental Mn, P, and S (Sigma-Aldrich, > 99% pure) were dried under vacuum before using them in solid-state reactions.
FTIR spectra were recorded on a ThermoFisher equipment with ATR. Scanning electron microscopy (SEM) was performed on the lamellar materials, using a Jeol scanning microscope (JSM-5410) with an Oxford Lin Isis energy dispersive X-ray detector (EDXS). The corresponding weight percentages obtained from EDXS were used to obtain the proposed stoichiometry, establishing three sulphur atoms per formula unit as reference, since the PS_3 ligand is not involved in the exchange reactions. Representative EDX spectra of the experimental results are shown in Figure S1. Lanthanides and manganese values have been obtained by ICP data, using a Perkin Elmer Avio 220 Max equipment. Seven standard solutions of Mn, Pr and Nd from 0.01 ppm to 20 ppm were prepared and analysed to obtain a reference line. Samples of the intercalated complexes dissolved in diluted nitric acid (10 ppm) were then analysed; measurements were repeated three times.
TGA curves were recorded with a Netzsch IRIS equipment, 209-F1 model under a nitrogen atmosphere with a 10 °C/min heating rate (Figure S2.). A Perkin Elmer Lambda 650 equipment coupled with an integration sphere was used to obtain the UV-visible solid state absorption spectra (Praying Mantis™ Diffuse Reflection Accessory and a “Sampling Kit”, model DRP-SAP, Harrick Scientific Products, Inc., New York, USA). The band gap values of the materials were obtained by the extrapolation of the linear zone in the Tauc plot. As the materials are derived from the $MnPS_3$ phase, which has an direct transition, $(\alpha h\nu)^2$ was used [36].

Powder X-ray diffraction data were collected on a Bruker D8 Advance diffractometer with Cu $K_{\alpha 1}$ radiation equipped with a LynxEye detector, in the range of 5° < 2θ< 60°. The data were analyzed by indexing the patterns through a Le Bail fit using the FullProf software [37] in the WinPLOTR interface [38].

The magnetic properties of the intercalation compounds were studied in the 2-300K temperature range, by *dc* measurements (zfc-fc show the same results), using a Quantum Design Dynacool Physical Properties Measurement System (PPMS), equipped with a vibrating sample magnetometer (VSM). Diamagnetic corrections were done using the following formula, $\mu_D = -(MW/2)10^{-6}$(emu mol^{-1}) [39]. The *ac* measurements were obtained with a Quantum Design SQUID magnetometer (MPMS XL7). The EPR spectra were recorded on a Bruker Elexsys E-580 spectrometer operating in the X-band at 9.442 GHz. The temperature was controlled by an ESR-900 continuous-flow liquid helium cryostat and an Oxford Instruments ITC 503 PID controller.

Syntheses

The macrocyclic complexes were obtained by the template reaction at room temperature with two different diamines, following procedures previously reported [30,40]. A solution of 2-hydroxy-5-methyl-1,3-benzenedicarbaldehyde (1 mmol in 50 mL of distilled acetonitrile (AN)) was slowly added to a lanthanide(III) nitrate solution (0.5 mmol in 30 mL AN), followed by the diamine (1mmol in 50 mL of AN), either 1,2-phenylenediamine for L^1H_2 and 1,3-diaminepropane for L^2H_2. Scheme 1 shows a simplified image of the complex, since the lanthanide ion is located above the plane of the ligand (Figure S5)[30].

The synthesis of the pristine phase was done by the ceramic method, using iodine to promote the reaction and crystallization of the product [41]. The elements, calculated to obtain 2 g of pristine phase, were ground jointly with 10 mg of iodine and sealed in glassy silica tubes under an argon atmosphere. After two weeks at 750 °C the solid was recovered as a microcrystalline powder, washed with carbon disulfide to remove the excess of iodine, followed by methanol, and dried under vacuum.

The potassium precursor (PP) was obtained by stirring a suspension of the pristine phase in a 2M potassium chloride solution for 24 hrs [18–21]. The obtained powder was washed with water and methanol, and dried under vacuum.

The intercalation of the lanthanide species was done by a microwave-assisted reaction. 150 mg of PP were suspended in a methanol solution of the lanthanide (III) nitrate or the corresponding complex (0.15 mmol, 80 mL). The suspension was irradiated with microwaves (800 W) for six minutes, using a LAVIS-1000 Multi-Quant microwave equipment with a frequency of 2459 MHz. The solid was filtered, washed with DMF and ethanol several times, and dried under vacuum before its characterization [19]. The stability of the macrocyclic complexes under microwave radiation was verified by the corresponding infrared spectra (Figure S3a.)

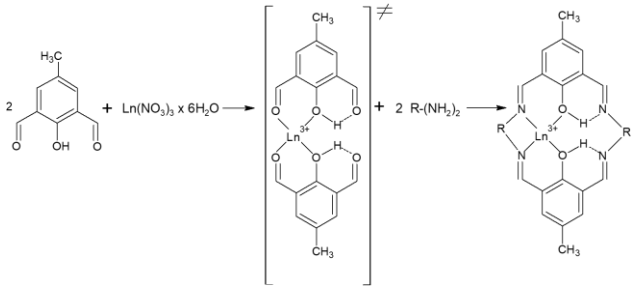

Scheme 1: Synthesis by the template reaction of the macrocyclic complexes. Nitrate ions and water molecules have been omitted for clarity. R is an aromatic ring $-(C_6H_4)-$ (OPDA for L^1H_2), or an aliphatic chain $-(CH_2)_3-$ (DAP for L^2H_2).

Acknowledgements

The authors thank Proyecto FONDECYT 1200033 and 11200919, CONICYT – FONDEQUIP/PPMS/EQM 130086 and French-Chilean International Research project entitled «Cooperation in Inorganic Chemistry» (IRP 2022-2026, CoopIC). The authors also acknowledge T. Guizouarn (Universite de Rennes 1, France) for the *ac* magnetic measurements; C. Daiguebonne and Ch. Blais for ICP data. ESS also thanks Financiamiento Basal, AFB180001 (CEDENNA). HE and CJM acknowledge funding by FAPESP, process number 2013/07793-6.

Keywords: Intercalated manganese(II) thiophosphate; lanthanides; magnetic properties; band gap energy.

References

1 R. Brec, *Solid State Ionics*, 1986, **22**, 3–30.

2 M. A. Susner, M. Chyasnavichyus, M. A. McGuire, P. Ganesh and P. Maksymovych, *Adv. Mater.*, 2017, **29**, 1602852.

3 L. Silipigni, A. Basile, F. Barreca, G. De Luca, L. Monsù Scolaro, B. Fazio and G. Salvato, *Philos. Mag.*, 2017, **97**, 2484–2495.

4 M. C. Friedel, *C. R. Acad. Sci.*, 1894, **119**, 260–264.

5 H. Falius, *Zeitschrift für Anorg. und Allg. Chemie*, 1968, **356**, 189–194.

6 W. Klingen, R. Ott and H. Hahn, *Zeitschrift für Anorg. und Allg. Chemie*, 1973, **396**, 271–278.

7 A. Le Méhauté, G. Ouvrard, R. Brec and J. Rouxel, *Mater. Res. Bull.*, 1977, **12**, 1191–1197.

8 C. Berthier, Y. Chabre and M. Minier, *Solid State Commun.*, 1978, 28, 327–332.

9 V. Grasso and L. Silipigni, *J. Opt. Soc. Am. B*, 1999, **16**, 132–136.

10 D. J. Goossens and T. J. Hicks, *J. Magn. Magn. Mater.*, 1998, **177**–**181**, 721–722.

11 P. Jeevanandam and S. Vasudevan, *J. Phys. Chem. B*, 1998, **102**, 4753–4758.

12 C. Sugiura, A. Kamata and S. Nakai, *J. Phys. Soc. Japan*, 1996, **65**, 2152–2157.

13 S. J. Price, D. O'Hare, R. J. Francis, A. Fogg and S. O'Brien, *Chem. Commun.*, 1996, 2453–2454.

14 A. R. Wildes, V. Simonet, E. Ressouche, G. J. McIntyre, M. Avdeev, E. Suard, S. A. J. Kimber, D. Lançon, G. Pepe, B. Moubaraki and T. J. Hicks, *Phys. Rev. B - Condens. Matter Mater. Phys.*, 2015, **92**, 1–11.

15 N. Ismail, M. Madian and A. A. El-Meligi, *J. Alloys Compd.*, 2014, **588**, 573–577.

16 A. Belianinov, V. Iberi, A. Tselev, M. A. Susner, M. A. McGuire, D. Joy, S. Jesse, A. J. Rondinone, S. V Kalinin and O. S. Ovchinnikova, *ACS Appl. Mater. Interfaces*, 2016, **8**, 7349–7355.

17 L. M. Schoop, R. Eger, R. K. Kremer, A. Kuhn, J. Nuss and B. V. Lotsch, *Inorg. Chem.*, 2017, **56**, 1121–1131.

18 P. Fuentealba, V. Paredes-Garcia, D. Venegas-Yazigi, I. D. A. Silva, C. J. Magon, R. Costa de Santana, N. Audebrand, J. Manzur and E. Spodine, *RSC Adv.*, 2017, **7**, 33305–33313.

19 P. Fuentealba, L. Serón, C. Sánchez, J. Manzur, V. Paredes-Garcia, N. Pizarro, M. Cepeda, D. Venegas-Yazigi and E. Spodine, *J. Coord. Chem.*, 2014, **67**, 3894–3908.

20 E. Spodine, P. Valencia-Gálvez, P. Fuentealba, J. Manzur, D. Ruiz, D. Venegas-Yazigi, V. Paredes-García, R. Cardoso-Gil, W. Schnelle and R. Kniep, *J. Solid State Chem.*, 2011, **184**, 1129–1134.

21 P. Fuentealba, C. Cortes, J. Manzur, V. Paredes-García, D. Venegas-Yazigi, I. D. A. Silva, R. C. De Santana, C. J. Magon and E. Spodine, *Dalt. Trans.*, 2017, **46**, 14373–14381.

22 L. Silipigni, G. Di Marco, G. Salvato and V. Grasso, *Appl. Surf. Sci.*, 2005, **252**, 1998–2005.

23 J. S. Miller and M. Drillon, Eds., *Magnetism: Molecules to Materials II*, Wiley-Vch, 2002.

24 J. S. O. Evans, D. O'Hare, R. Clement, A. Leaustic and P. Thuéry, *Adv. Mater.*, 1995, **7**, 735–739.

25 J. S. O. Evans, D. O'Hare and R. Clement, *J. Am. Chem. Soc.*, 1995, **117**, 4595–4606.

26 X. Zhang, H. Zhou, X. Su, X. Chen, C. Yang, J. Qin and M. Inokuchi, *J. Alloys Compd.*, 2007, **432**, 247–252.

27 Y. Wu and W. Bensch, *CrystEngComm*, 2010, **12**, 1003–1015.

28 P. Melnikov, I. V. Arkhangelsky, V. A. Nascimento, L. C. S. de Oliveira, W. Rodrigues Guimarães and L. Z. Zanoni, *J. Therm. Anal. Calorim.*, 2018, **133**, 929–934.

29 R. Decadt, P. Van Der Voort, I. Van Driessche, R. Van Deun and K. Van Hecke, *Acta Crystallogr. Sect. E Struct. Reports Online*, 2012, **68**, i59–i60.

30 R. C. de Santana, P. A. Fuentealba, L. J. Q. Maia, V. Paredes-García, D. Aravena, D. Venegas-Yazigi, J. Manzur and E. Spodine, *J. Lumin.*, 2018, **203**, 7–15.

31 W. Radecka-Paryzek, V. Patroniak and J. Lisowski, *Coord. Chem. Rev.*, 2005, **249**, 2156–2175.

32 I. Lagadic, P. G. Lacroix and R. Clément, *Chem. Mater.*, 1997, **9**, 2004–2012.

33 V. Grasso, F. Neri, L. Silipigni and M. Piacentini, *Nuovo Cim. D*, 1991, **13**, 633–645.

34 Y. . Köseglu, F. . Yildiz and B. . Aktas, *Nanostructured Materials and their Applications- NATO Science Series*, Kluwer Academic Publishers, 2004.

35 E. P. Papadopoulos, a. Jarrar and C. H. Issidorides, *J. Org. Chem.*, 1966, **31**, 615–616.

36 N. Kurita and K. Nakao, *J. Phys. Soc. Japan*, 1989, 58, 610–621.

37 J. Rodríquez-Carvajal and T. Roisnel, *Mater. Sci. Forum*, 2004, **443**–**444**, 123–126.

38 T. Roisnel and J. Rodríquez-Carvajal, *Mater. Sci. Forum*, 2001, **378**–**381**, 118–123.

39 G. A. Bain and J. F. Berry, *J. Chem. Educ.*, 2008, **85**, 532.

40 D. S. Kumar and V. Alexander, *Inorganica Chim. Acta*, 1995, **238**, 63–71.

41 K. Du, X. Wang, Y. Liu, P. Hu, M. I. B. Utama, C. K. Gan, Q. Xiong and C. Kloc, *ACS Nano*, 2016, **10**, 1738–1743.